JACS
JOURNAL OF THE AMERICAN CHEMICAL SOCIETY
pubs.acs.org/JACS
Article

Bonding and Suppression of a Magnetic Phase Transition in $EuMn_2P_2$

Tanya Berry,* Nicodemos Varnava, Dominic H. Ryan, Veronica J. Stewart, Riho Rasta, Ivo Heinmaa, Nitesh Kumar, Walter Schnelle, Rishi Bhandia, Christopher M. Pasco, N. P. Armitage, Raivo Stern, Claudia Felser, David Vanderbilt, and Tyrel M. McQueen

Cite This: *J. Am. Chem. Soc.* 2023, 145, 4527–4533
Read Online

ABSTRACT: Electrons in solids often adopt complex patterns of chemical bonding driven by the competition between energy gains from covalency and delocalization, and energy costs of double occupation to satisfy Pauli exclusion, with multiple intermediate states in the transition between highly localized, and magnetic, and delocalized, and nonmagnetic limits. Herein, we report a chemical pressure-driven transition from a proper Mn magnetic ordering phase transition to a Mn magnetic phase crossover in $EuMn_2P_2$ the limiting end member of the $EuMn_2X_2$ (X = Sb, As, P) family of layered materials. This loss of a magnetic ordering occurs despite $EuMn_2P_2$ remaining an insulator at all temperatures, and with a phase transition to long-range Eu antiferromagnetic order at $T_N \approx 17$ K. The absence of a Mn magnetic phase transition contrasts with the formation of long-range Mn order at $T \approx 130$ K in isoelectronic $EuMn_2Sb_2$ and $EuMn_2As_2$. Temperature-dependent specific heat and ^{31}P NMR measurements provide evidence for the development of short-range Mn magnetic correlations from $T \approx 250$–100 K, interpreted as a precursor to covalent bond formation. Density functional theory calculations demonstrate an unusual sensitivity of the band structure to the details of the imposed Mn and Eu magnetic order, with an antiferromagnetic Mn arrangement required to recapitulate an insulating state. Our results imply a picture in which long-range Mn magnetic order is suppressed by chemical pressure, but that antiferromagnetic correlations persist, narrowing bands and producing an insulating state.

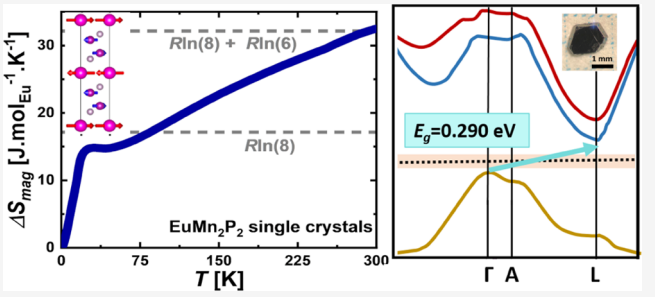

INTRODUCTION

The bonding in solids is often complex, driven by the ability of a multicomponent system to minimize interactions on different length scales through the formation of complex, emergent, states. This gives rise to a variety of exotic and useful electrical and magnetic properties, including charge and magnetic order, charge, and spin density waves, and superconductivity.[1−14] The precise ground-state configuration of electrons is determined by a subtle interplay between electron−nuclear and electron−electron interactions that is set by the local atomic bonding between atoms. When a material's structure has two distinct magnetic subunits, then the separation of energy scales within and between subunits can give rise to distinct behaviors that would not arise with a single homogeneous magnetic lattice. For example, the coexistence of magnetism and superconductivity in $Ho_2Ni_2B_2C$ arises due to localized 4f magnetism in HoC layers coupled to superconductivity in strongly covalently bonded Ni_2B_2 layers.[15] The interactions between subunits can be more directly coupled and depending on the balance of charge and spin interactions, drive subunits to different ground states. For example, the metal $EuFe_2As_2$, which crystallizes in the $ThCr_2Si_2$ crystal structure, exhibits separate magnetic ordering transitions for the anionic $(Fe_2As_2)^{2-}$ framework and cationic Eu^{2+} layers at ambient pressure.[16] Under chemical or epitaxial pressure, there is partial additional charge transfer to the $(Fe_2As_2)^{2-}$ framework, which results in superconductivity, with residual weak magnetism in the Eu layers.[16]

Separately, triangular lattices of magnetic ions have been intensively studied, with theoretical and experimental findings of classical and quantum spin liquid states that, in the language of chemistry, can best be viewed as the formation of dynamical long-range covalent bonded pairs.[17−21] In the classical limit, when the magnitude of the single atomic site electron spin is large and isotropic, more complex orders, such as the 120° state as found in $RbFe(MoO_4)_2$, results.[21] Similar to $RbFe(MoO_4)_2$, which has triangular layers of high-spin Fe^{3+} ($S = 5/2$), $EuMn_2X_2$ (X = Sb, As, P) crystallizes in a trigonal $CaAl_2Si_2$-type structure (space group $P\bar{3}m1$) and has triangular

Received: October 27, 2022
Published: February 15, 2023

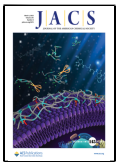

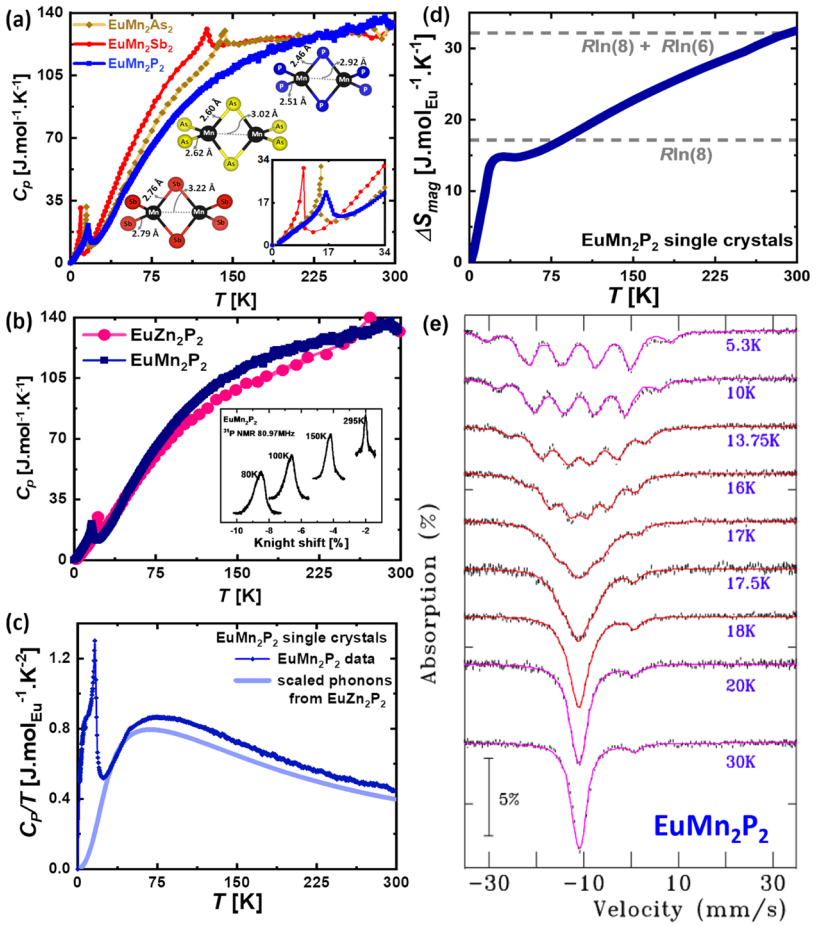

Figure 1. (a) Heat capacity as a function of temperature for $EuMn_2P_2$, $EuMn_2As_2$, and $EuMn_2Sb_2$ single crystals.[20,23] The phase transition close to $T \approx 20$ K is attributed to Eu magnetic order, while the phase transition close to $T \approx 130$ K is attributed to Mn order. Note that the transition attributed to Mn becomes less pronounced going from Sb to As and is absent for $EuMn_2P_2$. (b) Temperature-dependent heat capacity of $EuMn_2P_2$ and $EuZn_2P_2$ single crystals from $T = 2-300$ K. The sharp transition at $T_N = 17$ K in $EuMn_2P_2$ and $T_N = 21$ K in $EuZn_2P_2$ is attributed to Eu antiferromagnetic order. There is a broad region of excess entropy loss in $EuMn_2P_2$ from $T = 100-250$ K, suggesting the onset of Mn antiferromagnetic correlations. The inset shows ^{31}P NMR, suggesting the formation of a distribution of local magnetic fields on the timescale of the NMR experiment from $T = 150$ K to $T = 80$ K. (c) Change in magnetic entropy, integrated after subtracting the phonons from $T = 2-300$ K. (d) ΔS_{mag} from base to $T = 50$ K is close to the $R\ln(8)$ expected for an $L = S = 7/2$ system (i.e., Eu^{2+}) at $T = 17$ K, with an additional contribution from Mn at higher temperatures. (e) ^{151}Eu Mössbauer spectra of $EuMn_2P_2$ single crystals showing the evolution of the spectra with temperature. The solid lines are fits derived either from a full Hamiltonian solution (red line: $T = 13.75$ K) or from the dynamic model (magenta lines), showing the development of Eu order below $T = 17$ K.

layers of Eu^{2+} ($S = 7/2$).[22] These layers are, however, separated by triangular bilayers of nominally Mn^{2+} ions in $(Mn_2X_2)^{2-}$ polyanionic subunits. Given the strong covalent bonding expected between Mn and X, and the separation of magnetic energy scales between 3d and 4f magnetism, it is natural to ask: do the Eu and Mn triangular sublattices behave independently, or is there significant coupling between them? If the latter, how do the magnetic orders impact the electronic structure?

To answer these questions, in this work, we investigate the nature of bonding and magnetism in $EuMn_2P_2$ using a combination of thermodynamic, average, and local probes along with density functional theory (DFT) calculations. The $EuMn_2X_2$ (X = Sb, As, P) materials are chemically quite different from the $AEMn_2Pn_2$ (AE = alkali earth, Pn = Pnictogen) compounds since the alkali earth are nonmagnetic and do not interact with the magnetism with the Mn^{2+} spins. While $EuMn_2P_2$ has previously been reported as having magnetic Eu^{2+} cationic layers separated by nonmagnetic $(Mn_2P_2)^{2-}$ polyanionic subunits,[22] the property of Mn being nonmagnetic in $EuMn_2P_2$ is puzzling since isoelectronic $EuMn_2As_2$ and $EuMn_2Sb_2$ have a phase transition to long-range Mn magnetic order around $T \sim 130$ K.[22−25]

RESULTS AND DISCUSSION

Here, we report the discovery of hidden Mn antiferromagnetic correlations developing between $T = 250$ and 100 K via specific heat and ^{31}P NMR measurements. These short-range correlations are the behavior expected for a system that is transitioning to one with local covalent bonds. The total magnetic entropy associated with the Mn correlations is ~1/2 that is expected for full ordering and indicates the presence of significant magnetic fluctuations within the $(Mn_2P_2)^{2-}$ layers. No proper phase transition to static Mn order is observed from $T = 2$ K to $T = 700$ K. A-type Eu antiferromagnetic order develops below $T_N = 17$ K and does not seem to be significantly perturbed by the magnetic correlations on Mn, with a phase diagram similar to that of other Eu triangular lattice compounds. However, DFT calculations predict a large (35%, 0.16 eV) reduction in band gap with the development of

https://doi.org/10.1021/jacs.2c11324
J. Am. Chem. Soc. 2023, 145, 4527−4533

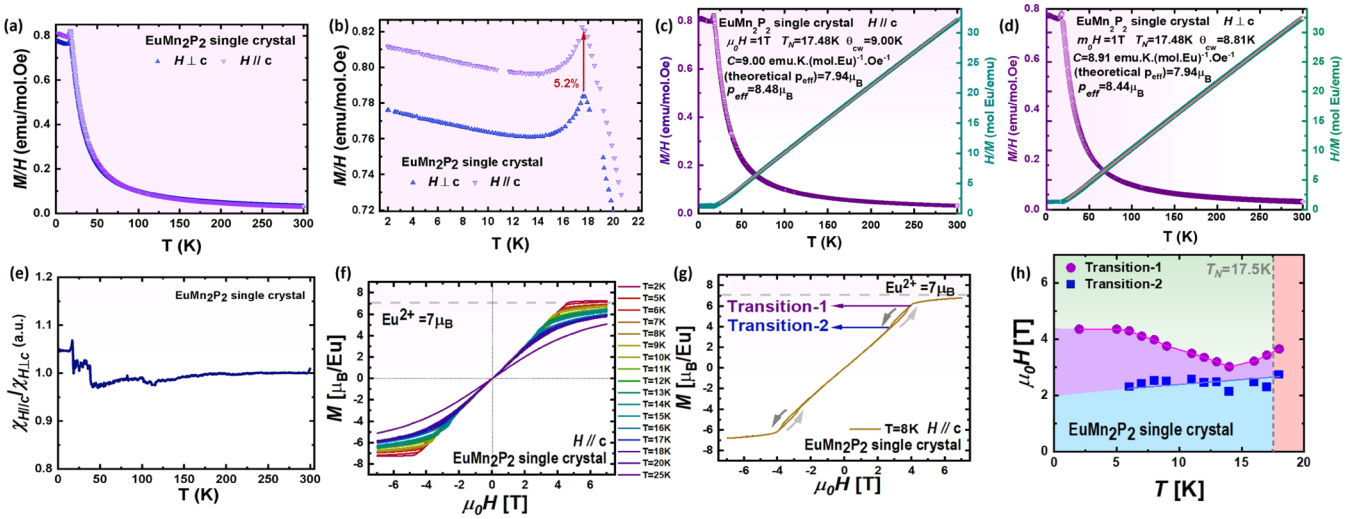

Figure 2. Magnetic behavior is isotopic above T_N for Eu with the development of a weak anisotropy (~5%) below T_N. (a) Comparison in the magnetization as a function of temperature for $\mu_oH\|c$ and $\mu_oH\perp c$, T = 2−300 K, (b) anisotropy in the $\mu_oH\|c$ and $\mu_oH\perp c$ below T_N, and (c) ratio of magnetization $\mu_oH\|c$ and $\mu_oH\perp c$ at μ_oH = 0.1 T and T = 2−300 K displaying the anisotropy below T_N (ref 1: $\chi(T_N)$ = 0.63 emu/mol). (c, d) Curie−Weiss analysis of $EuMn_2P_2$ for $\mu_oH\|c$ and $\mu_oH\perp c$ shows a cusp indicative of magnetic order at T_N = 17.5(1) K. The effective magnetic moment is higher than the theoretical value for Eu^{2+} (S = 7/2) and consistent with a small contribution from Mn ions. The measurements of the crystal sample show an excellent agreement with the previous study by Payne et al.[22] (e) Anisotropy that develops below T_N. (f) Magnetization as a function of magnetic field with $\mu_oH\|c$ from μ_oH = −7 to 7 T and T = 2−25 K, showing a linear response below 3 T, as seen in most Eu compounds.[22−25,27,28] Full saturation at 7 μ_B/Eu^{2+} is observed around μ_oH = 4 T. (g) Small, offset, hysteresis loops observed in the magnetization as a function of magnetic field with $\mu_oH\|c$ at intermediate temperatures below T_N, e.g., T = 8 K. These loops are observed between T = 6 and 20 K. (h) Eu magnetic phase diagram of $EuMn_2P_2$ derived from magnetization as a function of magnetic field at with $\mu_oH\|c$, constructed using the data from (a) and (b).

Eu magnetic order, attributed to an anomalously large exchange splitting of Mn-d-orbital derived conduction band states. Further, DFT calculations only predict an insulating state when Mn magnetic order is included and is antiferromagnetic. Our results imply a picture for $EuMn_2P_2$ in which long-range Mn magnetic order is suppressed by chemical pressure, but that antiferromagnetic correlations—a prelude to covalent bond formation—persist, narrowing bands and producing an insulating state. This raises the possibility of a novel fluctuating magnetic ground state in $EuMn_2P_2$,[26] as well as demonstrating a mechanism by which large exchange splittings of covalent conduction states can be produced in electronic structures by design.

Key evidence for Mn antiferromagnetic correlations and Eu magnetic order are shown in Figure 1. Literature-specific heat measurements for $EuMn_2As_2$ and $EuMn_2Sb_2$, Figure 1a, show two distinct phase transitions: one at $T_N \approx 20$ K associated with Eu ordering, and one at $T_N \approx 130$ K, associated with Mn ordering. In contrast, while $EuMn_2P_2$ shows a pronounced λ anomaly at $T_N \approx 17$ K with the development of Eu antiferromagnetic order, no anomaly indicative of a magnetic Mn phase transition is observed above T = 100 K.[23−25] Differential scanning calorimetry measurements up to T = 570 K (Figure S1) and magnetization measurements up to T = 700 K (Figure S2) also show no evidence for Mn magnetic ordering. One possible explanation for this lack of order would be electron delocalization and a transition to metallic behavior. However, temperature-dependent resistivity (Figure S3) and IR optical conductivity measurements (Figure S4) both indicate semiconducting/insulating behavior with electrical and optical gaps of 0.2 and 0.68 eV, respectively.

Comparison of the specific heat to the transition-metal-magnetic free analogue $EuZn_2P_2$, Figure 1b, reveals that there is a broad region, T = 100−250 K, where there is excess specific heat, and thus excess entropy, in $EuMn_2P_2$. ^{31}P NMR, Figure 1b, inset, and Figures S5 and S6, is in agreement with bulk magnetization and shows the development of distribution of local fields and suggestive of the development of Mn magnetic correlations below $T \approx 250$ K. Note that in ^{31}P NMR studies, the temperatures below 80 K were not studied due to the scarcity of helium, and the data show a monotonic decrease in the knight shifts. To quantify the magnitude of this excess contribution, an analytical model for the phonon-specific heat in $EuZn_2P_2$ was constructed and adjusted to account for the mass difference between Mn and Zn, Table SI and Figure 1c. Subtraction and integration yields magnetic entropy versus temperature, Figure 1d. The entropy recovered from base temperature to T = 50 K is 15 J mol^{-1} K^{-2}, close to the $R\ln(8)$ = 17.3 J mol^{-1} K^{-2} expected for ordering of Eu^{2+} (S = 7/2) ions. This interpretation, and the assignment of Eu as divalent Eu^{2+}, is further confirmed by ^{151}Eu Moessbauer and ZF-NMR, Figures 1e, S7, and S8, and Table SII, which shows development of Eu magnetic order below T_N = 17 K.

In the total entropy, however, there is then a gradual rise over T ~ 100−250 K to a value of approximately $R\ln(8)$ + $R\ln(6)$. This excess entropy cannot be from the Eu^{2+} ions, as they are L = 0 and there are no low-lying crystal field levels, and thus instead naturally attributed to magnetism on Mn. High-spin Mn would be S = 5/2, so we would expect an additional entropy recovery of $\Delta S_{mag} = 2R\ln(2S + 1) = 2R\ln(6)$ [there are two Mn ions per Eu ion]. This is about twice what is observed, suggesting that the Mn^{2+} is not rigorously high spin, that the Mn magnetic lattice is not fully magnetically ordered, or that a more exotic magnetic ground state (e.g., a quantum spin liquid) is present, all of which are in agreement with magnetization measurements (vide infra).

https://doi.org/10.1021/jacs.2c11324
J. Am. Chem. Soc. 2023, 145, 4527−4533

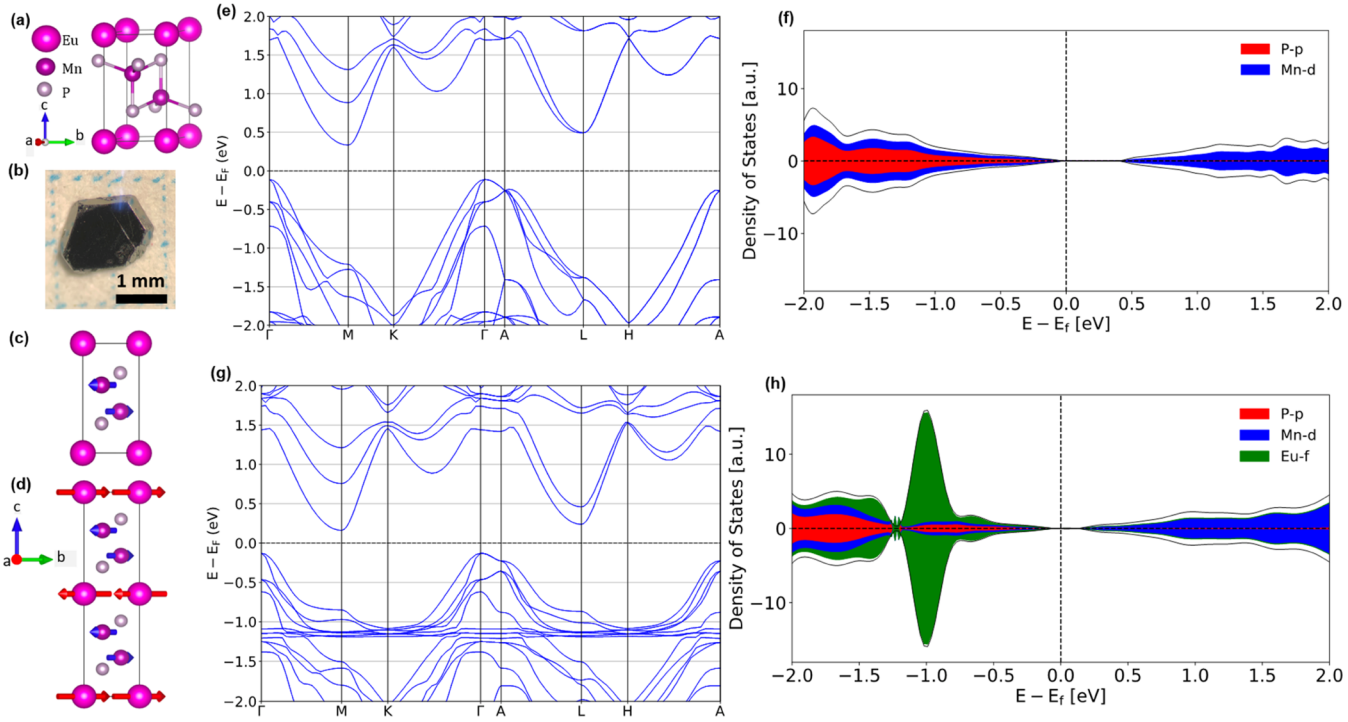

Figure 3. (a) $EuMn_2P_2$ crystallizes in space group $P\bar{3}m1$, no. 164. The crystal structure consists of anionic framework on $(Mn_2P_2)^{2-}$ with tetrahedral framework and Eu^{2+} cations occupying the corner sites. (b) Picture of grown single crystal of $EuMn_2P_2$. (c) Predicted intermediate-temperature magnetic structure with C-type antiferromagnetic order of Mn. (d) Predicted low-temperature magnetic structure with the same Mn ordering and A-type antiferromagnetic order of Eu and enlargement of the unit cell. (e) Electronic band structure and density of states within GGA + U following the magnetic structure as shown in (c). As expected from the bonding framework, the states near the Fermi level (E_f) are coming from Mn-d states, whereas the Eu-f states are further away from the E_f. Calculations with nonmagnetic Mn, or ferromagnetic Mn, predict a metallic/semimetallic state, at variance with experiment (see the Supporting Information). (f) Density of states (DOS) associated with the band structure in (d), showing a predicted band gap of 0.45 eV. (g) Electronic band structure and density of states within GGA + U following the magnetic structure as shown in (d), which includes Eu magnetic order. (h) DOS associated with the band structure in (f), showing a large exchange splitting reduction of the band gap to 0.29 eV.

Inspection of individual heating pulse traces showed no sign of latent heat that would indicate a first-order phase transition.

To explore the magnetic properties of $EuMn_2P_2$ in greater detail, magnetization as a function of temperature and magnetic field is shown in Figure 2. $M(T)$ plots show a clear antiferromagnetic phase transition at $T_N \approx 17$ K with a sharp peak in the magnetization followed by an unusual flat plateau below T_N, as seen in Figure 2a. We also observe signatures of anisotropy below T_N. It is easier to polarize the spins along the c-direction than the $a-b$ plane, which suggests that the c direction is the easy axis in $EuMn_2P_2$, Figure 2b. Figure 2c,d shows Curie−Weiss analysis of magnetic susceptibility for the two field directions. With $\mu_0 H \| c$, a Curie constant per formula unit of $C = 9.0$ emu K mol·f.u.$^{-1}$ Oe^{-1} and a positive Weiss temperature of 9.0 K are found. The Curie constant is larger than the expected value for pure high-spin Eu^{2+} ($S = 7/2$), $C = 7.8$ emu K mol·f.u.$^{-1}$ Oe^{-1}, suggesting a contribution of ∼1 emu K mol·f.u.$^{-1}$ Oe^{-1} from Mn. This is much less than the extra 2·4.3−8.6 emu K mol·f.u.$^{-1}$ Oe^{-1} that would be expected from high-spin Mn^{2+}. It is, however, consistent with the strong covalent bonds in the Mn−P framework that are known to reduce magnetic moments[27] and suggestive of the existence of Mn antiferromagnetic correlations over the region of the fit, $T = 50-300$ K. With $\mu_0 H \perp c$, similar values are found: a Curie constant per formula unit of $C = 8.91$ emu K mol·f.u.$^{-1}$ Oe^{-1} and a positive Weiss temperature of 8.8 K are found. This is consistent with an isotropic magnetic response above the Eu ordering temperature, Figure 2e. The Mn contributions from Curie−Weiss analysis are also not seen in $SrMn_2P_2$ and $CaMn_2P_2$. The $M(H)$ behavior in the low-temperature region with $\mu_0 H \| c$ is shown in Figure 2f. Below T_N, the magnetization is nearly linear with applied magnetic field until saturation is reached. Such behavior is seen in many Eu compounds.[20−25,27−29] No excess magnetization attributable to Mn is observed. This implies that Mn has strong antiferromagnetic correlations. More detailed inspection shows that there are small but systematic "open" hysteresis loops that appear prior to saturation, Figure 2g. There are two noticeable attributes to this result: (a) this plot is reproducible, (b) it follows a behavior one would expect for a ferromagnetic-type state. These results are consistent with an antiferromagnetic ground state at zero field that arises from coupled ferromagnetic planes of Eu^{2+} ions. This agrees with previous findings from neutron diffraction.[22] Figure 2h summarizes the magnetic phase diagram extracted from these data.

We use density functional theory (DFT) within GGA + U to explore the electronic structure and bonding of $EuMn_2P_2$ and how it might be impacted by the observed magnetic behaviors. $EuMn_2P_2$ crystallizes in a trigonal lattice (Tables SIII−SV and Figure 3a). Calculations with A-type antiferromagnetic order and a Hubbard U (to account for the strong Pauli repulsion in open shell f systems) on the Eu atoms, to match known Eu magnetic behavior,[22] and along with nonmagnetic Mn predicts metallic behavior, in disagreement with experiment. Indeed,

https://doi.org/10.1021/jacs.2c11324
J. Am. Chem. Soc. 2023, 145, 4527−4533

the Mn d-orbitals dominate the Fermi level, Figure S9a, as expected for Mn, which has a partly filled d-orbital manifold. However, introducing magnetism on Mn by either setting an antiferromagnetic Mn order without a Hubbard U or Mn ferromagnetic order with a Hubbard U also results in metallic behavior (Figure S10). It is only when a Hubbard U and antiferromagnetic order on the Mn ions is included that semiconducting behavior is predicted, Figure 2c,e,f. Inclusion of spin−orbit coupling (SOC), Figure S11, has a negligible effect on the band structure and symmetry analysis confirms that the compound is a topologically trivial insulator. These results suggest that the band narrowing associated with Mn antiferromagnetic exchange plays a pivotal role in opening a band gap—this is exactly the behavior expected to occur in the formation of covalent metal−metal bonds and suggests that $EuMn_2P_2$ is on the verge of forming such bonds.

As the states near E_f are dominated by Mn in the $(Mn_2P_2)^{2-}$ layers, this necessitates a proper understanding of the behavior of Mn. By computing the energy of different antiferromagnetic configurations, we can use DFT to predict the intermediate-temperature and low-temperature magnetic configurations of this material, including both Mn and Eu magnetism. Since the SOC is negligible, we consider A-type, C-type, and G-type antiferromagnetic configurations for Mn. For the intermediate-temperature configuration, we set the Eu f-orbitals in the core and we find that the C-type configuration, Figure S12, is the lowest in energy. Such assignment is in agreement with the observation of a sharp magnetic phase transition when Eu orders below T = 17 K because of lowering in the symmetry that would be predicted when Eu orders. In contrast, the close-in-energy G-type Mn order would have resulted in a crossover instead of transition for Eu magnetic ordering, as there would no longer be a change in symmetry. The C-type magnetic structure for Mn is also observed in the isostructural analogue $EuMn_2As_2$, and thus this arrangement likely best describes the local ordering in $EuMn_2P_2$.[23−25]

The corresponding band structure and density of states with Mn magnetic order and Eu in the core, Figure 2e,f, give a small indirect band gap, ∼0.45 eV. This indirect gap decreases significantly to ∼0.29 eV when Eu magnetic order is considered due to exchange splitting of the conduction band states, Figures 2g,h and S9b. In both cases, the direct gap is markedly larger, ∼1.3 eV. These gaps agree with room-temperature optical reflectivity measurements, Figure S4, which shows a tail of absorption down to ∼0.2 eV with a sharp edge at ∼0.7 eV, and also in agreement with temperature-dependent resistivity measurements, Figure S3. Such a large change in indirect gap, with a correspondingly large splitting of conduction band states at the conduction minimum, would be expected to give rise to novel electrical behavior, and in particular nonlinear IV curves, Figure S13. And indeed, there is development of a nonlinear IV response close to the Eu magnetic ordering transition, Figures S14−S17, Tables SVI, and SVII. However, thermomagnetoelectric finite element simulations with realistic materials parameters and dimensions, Figure S18, show that the nonlinearity likely arises due to Joule heating, and is not directly associated with changes in the intrinsic electronic structure and bonding.

It is natural to ask why $EuMn_2P_2$ behaves differently from $EuMn_2As_2$ and $EuMn_2Sb_2$. Not only does the former not show a proper Mn magnetic phase transition, but the latter are found to exhibit metallic (or very heavily doped semiconductor) conductivity. The bond distances between Mn−X (X = P, As, and Sb) increase as the ionic radius of X becomes larger, Figure 1a. Combined with an increase in the difference in electronegativity, this reduces the covalency of the $(Mn_2X_2)^{2-}$ network and results in more "ionic" behavior from the Mn cations, Table SVIII. This explains the more definitive magnetic transitions from X = P to As and Sb. At the same time, the valence and conduction bands become broader going from X = P to X = Sb due to larger orbitals on the anions, which reduces the gap and explains the higher metallicity.

CONCLUSIONS

In summary, we report the discovery of suppression of a long-range magnetic ordering phase transition in favor of a crossover with the development of Mn antiferromagnetic correlations in $EuMn_2P_2$. The property Mn not having a phase transition in $EuMn_2P_2$ is surprising since isoelectronic $EuMn_2As_2$ and $EuMn_2Sb_2$ have Mn magnetic order phase transitions, but can be understood as chemical pressure favoring local antiferromagnetic correlations that are prelude to the formation of proper metal−metal covalent bonds. We also predict that there is a substantial exchange splitting of $(Mn_2P_2)^{2-}$ states with the occurrence of Eu magnetic order. Our results provide evidence for rich bonding and changes in electron behavior in $EuMn_2P_2$ and should open avenues to study other Mn materials for realizing complex bonding between covalent and magnetic orders.

ASSOCIATED CONTENT

Data Availability Statement

Experimental data files are available upon reasonable request from the corresponding author.

Supporting Information

The Supporting Information is available free of charge at https://pubs.acs.org/doi/10.1021/jacs.2c11324.

Materials and methods, differential scanning calorimetry, $M(T)$ for T = 300−700 K, temperature-dependent resistivity, FT-IR spectra, shift susceptibility, ^{31}P T_1 and T_2 times, phonon model parameters, ^{151}Eu Mössbauer hyperfine field temperature dependence, ^{153}Eu ZF-NMR, ZF-NMR Hamiltonian fit parameters, single-crystal structure determination, density of states calculations yielding semiconducting behavior, density of states calculations yielding metallicity, effect of spin−orbit coupling, magnetic order energetics, predicted IV behavior due to exchange splitting, measured IV behavior summary, dV/dI vs V curves, analysis of variable range hopping for 0 T, two-channel model fit parameters at 0 T, analysis of variable range hopping for 9 T, two-channel model fits parameters at 9 T, ansys finite element simulations, and table of Mn−P bond lengths (PDF)

AUTHOR INFORMATION

Corresponding Author

Tanya Berry − *Department of Chemistry, The Johns Hopkins University, Baltimore, Maryland 21218, United States; Institute for Quantum Matter, William H. Miller III Department of Physics and Astronomy, The Johns Hopkins University, Baltimore, Maryland 21218, United States; Department of Chemistry, Princeton University, Princeton, New Jersey 08540, United States;* orcid.org/0000-0002-1583-2120; Email: tberry@ucdavis.edu

https://doi.org/10.1021/jacs.2c11324
J. Am. Chem. Soc. 2023, 145, 4527−4533

Authors

Nicodemos Varnava − *Department of Physics & Astronomy, Rutgers University, Piscataway, New Jersey 08854, United States*

Dominic H. Ryan − *Physics Department and Centre for the Physics of Materials, McGill University, Montreal, Quebec H3A 2T8, Canada*

Veronica J. Stewart − *Department of Chemistry, The Johns Hopkins University, Baltimore, Maryland 21218, United States; Institute for Quantum Matter, William H. Miller III Department of Physics and Astronomy, The Johns Hopkins University, Baltimore, Maryland 21218, United States;* orcid.org/0000-0002-9347-4998

Riho Rasta − *National Institute of Chemical Physics and Biophysics, 12618 Tallinn, Estonia*

Ivo Heinmaa − *National Institute of Chemical Physics and Biophysics, 12618 Tallinn, Estonia*

Nitesh Kumar − *Max-Planck-Institute for Chemical Physics of Solids, D-01187 Dresden, Germany;* orcid.org/0000-0002-2274-5041

Walter Schnelle − *Max-Planck-Institute for Chemical Physics of Solids, D-01187 Dresden, Germany*

Rishi Bhandia − *Institute for Quantum Matter, William H. Miller III Department of Physics and Astronomy, The Johns Hopkins University, Baltimore, Maryland 21218, United States*

Christopher M. Pasco − *Department of Chemistry, The Johns Hopkins University, Baltimore, Maryland 21218, United States; Institute for Quantum Matter, William H. Miller III Department of Physics and Astronomy, The Johns Hopkins University, Baltimore, Maryland 21218, United States;* orcid.org/0000-0003-3837-6858

N. P. Armitage − *Institute for Quantum Matter, William H. Miller III Department of Physics and Astronomy, The Johns Hopkins University, Baltimore, Maryland 21218, United States*

Raivo Stern − *National Institute of Chemical Physics and Biophysics, 12618 Tallinn, Estonia;* orcid.org/0000-0002-6724-9834

Claudia Felser − *Max-Planck-Institute for Chemical Physics of Solids, D-01187 Dresden, Germany*

David Vanderbilt − *Department of Physics & Astronomy, Rutgers University, Piscataway, New Jersey 08854, United States*

Tyrel M. McQueen − *Department of Chemistry, The Johns Hopkins University, Baltimore, Maryland 21218, United States; Institute for Quantum Matter, William H. Miller III Department of Physics and Astronomy and Department of Materials Science and Engineering, The Johns Hopkins University, Baltimore, Maryland 21218, United States;* orcid.org/0000-0002-8493-4630

Complete contact information is available at: https://pubs.acs.org/10.1021/jacs.2c11324

Funding

This research was conducted at the Institute of Quantum Matter, an Energy Frontier Research Center funded by the U.S. Department of Energy Office of Science, Basic Energy Sciences, under Award No. DE-SC001933. T.B. acknowledges support from NSF-MRSEC through the Princeton Center for Complex Materials NSF-DMR-2011750. Financial support for this work was provided by Fonds Qu'eb'eco de la Recherche sur la Nature et les Technologies, and the Natural Sciences and Engineering Research Council (NSERC) Canada. Work in Tallinn was funded by the European Regional Development Fund (Awards TK133 and TK134) and the Estonian Research Council (Projects PRG4 and IUT23−7). This work was also financially supported by the European Research Council (ERC Advanced Grant No. 742068 "TOPMAT"). The authors also acknowledge funding by the DFG through SFB 1143 (project ID. 247310070) and the Würzburg-Dresden Cluster of Excellence on Complexity and Topology in Quantum Matter ct.qmat (EXC2147, project ID. 39085490).

Notes

The authors declare no competing financial interest.

■ ACKNOWLEDGMENTS

The authors acknowledge Collin L. Broholm, Mazhar Ali, Johannes Gooth, Defa Lui, Vincent Morano, Shannon Bernie, Maxime Siegler, Johnathan Tuck, and Rauf Koban for helpful discussions.

■ REFERENCES

(1) Iga, F.; Shimizu, N.; Takabatake, T. Single crystal growth and physical properties of Kondo insulator YbB_{12}. *J. Magn. Magn. Mater.* **1998**, *177*−*181*, 337−338.

(2) Nagatsuma, T.; Ducournau, G.; Renaud, C. Advances in terahertz communications accelerated by photonics. *Nat. Photon* **2016**, *10*, 371−379.

(3) Nesper, R. The Zintl-Klemm concept−a historical survey. *Z. Anorg. Allg. Chem.* **2014**, *640*, 2639−2648.

(4) Bonville, P.; Rullier-Albenque, F.; D Colson, D. A Forget, Incommensurate spin density wave in Co-doped $BaFe_2As_2$. *Europhys. Lett.* **2010**, *89*, No. 67008.

(5) Gooth, J.; Bradlyn, B.; Honnali, S.; Schnindler, C.; Kumar, N.; Noky, J.; Qi, Y.; Shekhar, C.; Sun, Y.; Wang, Z.; Bernevig, B. A.; Felser, C. Axionic charge-density wave in the Weyl semimetal $(TaSe_4)_2I$. *Nature* **2019**, *575*, 315−319.

(6) Moll, P. J. W.; Kushwaha, P.; Nandi, N.; Schmidt, B.; Mackenzie, A. P. Evidence for hydrodynamic electron flow in $PdCoO_2$. *Science* **2016**, *351*, 1061−1064.

(7) Toberer, E. S.; May, A. F.; Snyder, G. J. Zintl chemistry for designing high efficiency thermoelectric materials. *Chem. Mater.* **2010**, *22*, 624−634.

(8) Devarakonda, A.; Inoue, H.; Fang, S.; Ozsoy-Keskinbora, C.; Suzuki, T.; Kriener, M.; Fu, L.; Kaxiras, E.; Bell, D.; Checkelsky, J. Clean 2D superconductivity in a bulk van der Waals superlattice. *Science* **2020**, *370*, 231.

(9) Ortiz, B. R.; Sarte, P. M.; Kenney, E. M.; Graf, M. J.; Teicher, S. M. L.; Seshadri, R.; Wilson, S. D. Superconductivity in the $Z2$ kagome metal KV_3Sb_5. *Phys. Rev. Mater.* **2021**, *5*, No. 034801.

(10) Berry, T.; Nicklas, M.; Yang, Q.; Schnelle, W.; Wawrzyńczak, R.; Förster, T.; Gooth, J.; Felser, C.; McQueen, T. M. Bonding and Electronic Nature of the Anionic Framework in $LaPd_3S_4$. *Chem. Mater.* **2022**, *34*, 10390−10398.

(11) Sinha, M.; Vivanco, H. K.; Wan, C.; Siegler, M. A.; Stewart, V. J.; Pogue, E. A.; Pressley, L. A.; Pressley, L. A.; Berry, T.; Berry, T.; Wang, Z.; Wang, Z.; Johnson, I.; Johnson, I.; Chen, M.; Chen, M.; Tran, T. T.; Tran, T. T.; Phelan, W. A.; Phelan, W. A.; McQueen, T. M. Twisting of 2D Kagome Sheets in Layered Intermetallics. *ACS Cent. Sci.* **2021**, *7*, 1381−1390.

(12) Yu, Y.; Ma, L.; Cai, P.; Zhong, R.; Ye, C.; Shen, J.; Gu, G. D.; Chen, X. H.; Zhang, Y. High-temperature superconductivity in monolayer $Bi_2Sr_2CaCu_2O_{8+\delta}$. *Nature* **2019**, *575*, 156−163.

(13) Guillamón, I.; Suderow, H.; Vieira, S.; Cario, L.; Diener, P.; Rodière, P. Superconducting density of states and vortex cores of 2H-NbS_2. *Phys. Rev. Lett.* **2008**, *101*, No. 166407.

(14) Alexandradinata, A.; Wang, C.; Duan, W.; Glazman, L. Revealing the topology of Fermi-surface wave functions from magnetic quantum oscillations. *Phys. Rev. X* **2018**, *8*, No. 011027.

(15) Yamanaka, S. Silicon clathrates and carbon analogs: high pressure synthesis, structure, and superconductivity. *Dalton Trans.* **2010**, *39*, 1901−1915.
(16) Jeevan, H. S.; Hossain, Z.; Kasinathan, D.; Rosner, H.; Geibel, C.; Gegenwart, P. High-temperature superconductivity in $Eu_{0.5}K_{0.5}Fe_2As_2$. *Phys. Rev. B* **2008**, *78*, No. 092406.
(17) Broholm, C.; Cava, R. J.; Kivelson, S. A.; Nocera, D. G.; Norman, M. R.; Senthi, T. Quantum spin liquids. *Science* **2020**, *367*, No. eaay0668.
(18) Savary, L.; Balents, L. Quantum spin liquids: a review. *Rep. Prog. Phys.* **2017**, *80*, No. 016502.
(19) Zhu, Z.; Maksimov, P. A.; White, S. R.; Chernyshev, A. L. Topography of spin liquids on a triangular lattice. *Phys. Rev. Lett.* **2018**, *120*, No. 207203.
(20) Paddison, J. A. M.; Daum, M.; Dun, Z.; Ehlers, G.; Liu, Y.; Stone, M. B.; Zhou, H.; Mourigal, M. Continuous excitations of the triangular-lattice quantum spin liquid $YbMgGaO_4$. *Nat. Phys.* **2017**, *13*, 117−122.
(21) Svistov, L. E.; Smirnov, A. I.; Prozorova, L. A.; Petrenko, O. A.; Micheler, A.; Büttgen, N.; Shapiro, A. Y.; Demianets, L. N. Magnetic phase diagram, critical behavior, and two-dimensional to three-dimensional crossover in the triangular lattice antiferromagnet $RbFe(MoO_4)_2$. *Phys. Rev. B* **2016**, *74*, No. 024412.
(22) Payne, A. C.; Sprauve, A. E.; Olmstead, M. M.; Kauzlarich, S. M.; Chan, J. Y.; Reisner, B. A.; Lynn, J. W. Synthesis, magnetic and electronic properties of single crystals of $EuMn_2P_2$. *J. Solid State Chem.* **2002**, *163*, 498−505.
(23) Anand, V. K.; Johnston, D. C. Metallic behavior induced by potassium doping of the trigonal antiferromagnetic insulator $EuMn_2As_2$. *Phys. Rev. B* **2016**, *94*, No. 014431.
(24) Dahal, A.; Chen, Y.; Heitmann, T.; Thamizhavel, A.; Paramanik, U.; Dhar, S. K.; Singh, D. K. Spin correlation in trigonal $EuMn_2As_2$. *Phys. Rev. B* **2019**, *99*, No. 085135.
(25) Schellenberg, I.; Eul, M.; Hermes, W.; Pöttgen, R. A ^{121}Sb and ^{151}Eu Mössbauer Spectroscopic Investigation of $EuMn_2Sb_2$, $EuZn_2Sb_2$, $YbMn_2Sb_2$, and $YbZn_2Sb_2$. *Z. anorg. allg. Chem.* **2010**, *636*, 85−93.
(26) Roberg, M.; Reveyrand, T.; Ramos, I.; Falkenstein, E. A.; Popovic, Z. High Efficiency Harmonically Terminated Diode and Transistor Rectifiers. *IEEE Trans. Microwave Theory Technol.* **2012**, *60*, 4043−4052.
(27) Berry, T.; Stewart, V. J.; Redemann, B. W. Y.; Lygouras, C.; Varnava, N.; Vanderbilt, D.; McQueen, T. M. A-type antiferromagnetic order in the Zintl-phase insulator $EuZn_2P_2$. *Phys. Rev. B* **2022**, *106*, No. 054420.
(28) Varnava, N.; Berry, T.; McQueen, T. M.; Vanderbilt, D. Engineering magnetic topological insulators in $Eu_5M_2X_6$ Zintl compounds. *Phys. Rev. B* **2022**, *105*, No. 235128.
(29) Berry, T.; Parkin, S. R.; McQueen, T. M. Antiferro- and Metamagnetism in the $S = 7/2$ Hollandite Analog $EuGa_2Sb_2$. *Phys. Rev. Mater.* **2021**, *5*, No. 114401.

https://doi.org/10.1021/jacs.2c11324
J. Am. Chem. Soc. 2023, 145, 4527−4533